American Mineralogist, Volume 82, pages 772–780, 1997

Monazite-xenotime thermobarometry: Experimental calibration of the miscibility gap in the binary system $CePO_4$-YPO_4

RENÉ GRATZ AND WILHELM HEINRICH

GeoForschungsZentrum Potsdam, Department of Experimental Petrology,
P.O. Box 60 07 51, D-14407 Potsdam, Germany

ABSTRACT

Solid solutions of $(Ce,Y)PO_4$ were synthesized hydrothermally between 300 °C and 1000 °C at pressures of 2, 5, 10, and 15 kbar. Experiment products were analyzed by electron microprobe, and their lattice parameters were refined by Rietveld analysis of XRD powder patterns. Over a wide range of bulk compositions, two immiscible phases formed: monazite with a $P2_1/n$ structure ($REEO_9$ polyhedron) and xenotime with an $I4_1/amd$ structure ($REEO_8$ polyhedron). Variations of the unit-cell dimensions are directly correlated with variations in composition. The boundaries of the asymmetric miscibility gap are strongly dependent on temperature. At 2 kbar and from 300–1000 °C, maximum Y concentrations in monazite coexisting with xenotime increase from 3–16 mol%. With increasing pressure, this limb is shifted to higher Y contents so that at 15 kbar it ranges from 6 to about 25 mol% for the same temperature range. In contrast, Ce concentrations in xenotime do not exceed 3 mol% at 1000 °C over the entire pressure range. Our experimentally determined boundaries fit surprisingly well with empirical calibrations of the (LREE-HREE,Y)PO_4-solvus boundaries derived from a suite of low pressure metapelites (3 to 5 kbar) that equilibrated at peak temperatures ranging from 400–700 °C. The behavior of the natural $(REE,Y)PO_4$ system is probably well described by the simple $(Ce,Y)PO_4$ binary, at least for metapelitic compositions. Many natural samples of monazite coexisting with xenotime show prograde growth zonation with respect to the incorporation of HREE + Y. The combination of our thermometer along with U-Pb and Sm-Nd age determinations of high spatial resolution may thus provide information about prograde branches of metamorphic *PTt* paths.

INTRODUCTION

The REE-orthophosphate minerals monazite and xenotime occur together in many metamorphic rocks on thin section scale, and they are common accessory minerals in metapelites that formed from greenschist to granulite facies conditions. Monazite preferentially incorporates the light rare earth elements (LREE), and xenotime, incorporates the heavy rare earth elements (HREE) and Y (Franz et al. 1996; Heinrich et al. 1997). The structural properties at 25° C and 1 bar of pure REE phosphates along the entire REE series and YPO_4 have been presented by Ni et al. (1995, Fig. 1). Pure $REEPO_4$ phases of the larger LREE from $LaPO_4$ to $GdPO_4$ have a monoclinic monazite structure with the space group $P2_1/n$ and a ninefold coordination for the REE. Phosphates that incorporate the smaller HREE from $TbPO_4$ to $LuPO_4$ and YPO_4 are isostructural with zircon, with the space group $I4_1/amd$ and, with a regular $REEO_8$ polyhedron. Both structures have isolated phosphate tetrahedra separated by intervening $REEO_x$ polyhedra. Both series also show a linear correlation between cell volume and ionic radius of their respective REE. The cell volume of the monazite suite decreases from 305.7 Å^3 ($LaPO_4$) to 279.1 Å^3 ($GdPO_4$) as the ionic radii decrease from 1.216 (La) to 1.107 Å (Gd), while that of the xenotime suite decreases from 291.1 Å^3 ($TbPO_4$) to 273.6 Å^3 ($LuPO_4$) as the radii decrease from 1.04 for Tb to 0.985 Å for Lu (Fig. 1; values from Ni et al. 1995). At conditions of 25 °C and 1 bar, the transition from the monazite to the xenotime structure occurs between the $GdPO_4$ and $TbPO_4$ phases (Fig. 1).

In igneous and metamorphic rocks, the entire compositional range of REE + Y is present and coexisting monazite and xenotime form, to some extent, solid solutions. Because of their different structures a miscibility gap in the LREE (HREE,Y) system must exist. The compositions of the two coexisting phosphate phases depend both on bulk composition and on the distribution coefficients of each REE and Y between the two, both of which are also pressure and temperature dependent. Such REE distribution coefficients between monazite and xenotime were determined empirically from a suite of metapelites that equilibrated between about 400–700 °C at pressures from 3 to 5 kbar (Heinrich et al. 1997). The major element concentrations of both phases in all the samples were very similar and typical for metapelites and did not depend on metamorphic grade. Monazite consisted mainly of La, Ce, and Nd $(La_{0.20\text{-}0.23}, Ce_{0.41\text{-}0.45}, Nd_{0.15\text{-}0.18})PO_4$

0003–004X/97/0708–0772$05.00

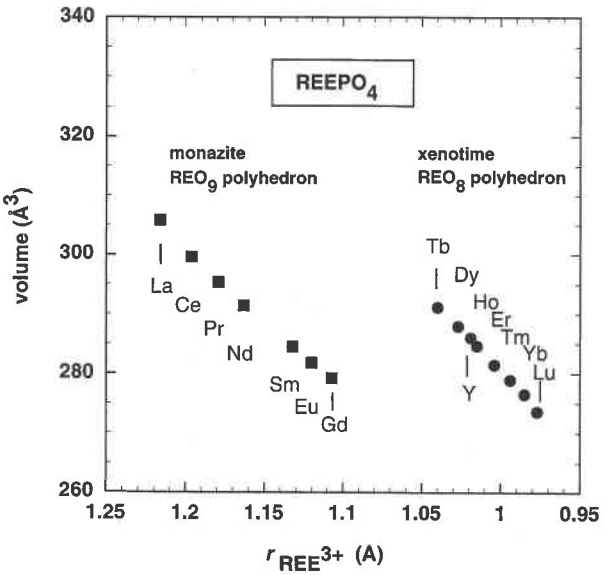

FIGURE 1. Unit-cell volumes of pure $REEPO_4$ phases vs. REE ionic radii, redrawn from Ni et al. (1995). The value of $r(REE^{3+})$ is the effective radius in ninefold and eightfold coordination in monazite and xenotime structure, respectively (Shannon 1976).

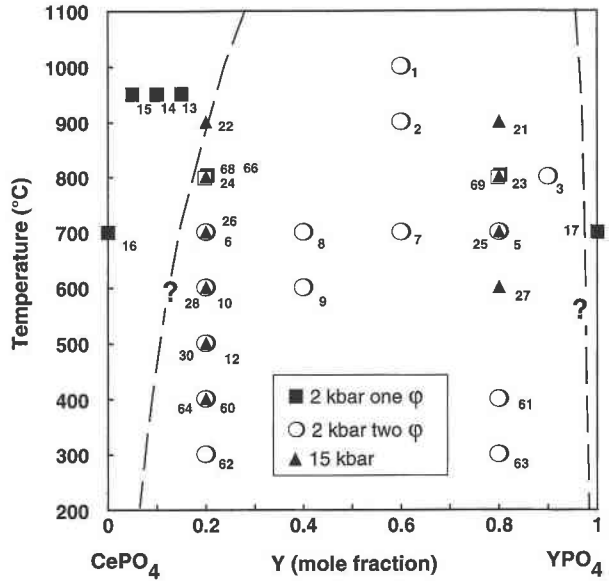

FIGURE 2. X_Y vs. temperature plot of the experimental setup. Numbers denote temperature, pressure, and bulk composition of each experiment. Black squares yielded single-phase products. Open circles and black triangles at 2 and 15 kbar yielded two solid phases. Experiments 66, 68, and 69 (open squares) show experiments at 5 and 10 kbar. Also given are the tentative boundaries of the miscibility gap.

with all other elements below 6 mol%. Xenotime consisted mainly of YPO_4 with some Dy and Gd solid solutions ($Y_{0.76-0.80}$, $Dy_{0.05-0.07}$, and $Gd_{0.04-0.06}$). Gd was preferentially partitioned into xenotime by a factor of two to four and was thus considered as an HREE, despite the fact that pure $GdPO_4$ crystallizes in monazite structure (Fig. 1).

In contrast, the minor HREE concentrations in monazite increased strongly with increasing metamorphic grade. The sum Y+Dy+Gd increased from about 3–10 mol% from 400–700 °C. Similarly, Sm and Nd in xenotime increased by a factor of three to four with increasing metamorphic grade, but their total amount did not exceed 1 mol% at high temperatures. The $X_{HREE,Y}$ in monazite and X_{LREE} in xenotime for seven metapelites defined two limbs along a strongly asymmetric miscibility gap with the monazite limb, particularly, showing a significant temperature dependence.

The aim of this study was to determine experimentally the pressure and temperature dependence of the boundaries of the monazite–xenotime miscibility gap in the range of 300–1000 °C and 2 to 15 kbar. We have chosen the simple binary $CePO_4$-YPO_4 as a model system and propose to show that this simplified system describes the immiscibility behavior of complex metapelite bulk phosphate compositions adequately. Finally, we emphasize the usefulness of the monazite-xenotime geothermobarometer along with some speculations on how *P-T* data derived from monazite-xenotime compositions could directly be linked to U-Pb and Sm-Nd age determinations of the same minerals, and stress the feasibility of the REE phosphates for determining *PTt* paths in metamorphic rocks.

EXPERIMENTAL AND ANALYTICAL METHODS

Starting materials and synthesis of phosphates

Pure CeO_2 and Y_2O_3 (99.99% purity, Fluka Chemicals) were mixed in various ratios and homogenized by grinding in an agate mortar. These mixtures were placed in gold capsules along with solid orthophosphoric acid (H_3PO_4, 98% purity, Haereus Chemicals) and 5 to 10 μL of distilled water. The amount of solid H_3PO_4 exceeded the stoichiometric value by about 30%. With the preparation technique described here it is impossible to add an exact amount of solid H_3PO_4 because the substance is extremely hygroscopic. For experiments in cold-seal vessels, welded capsules were 20 mm long, 3 mm in diameter, with walls 0.2 mm thick, and contained about 50 mg of oxide mix. Welded capsules for piston-cylinder experiments were 10 mm long and contained about 20 mg of oxide mix. Capsules were checked for leaks by heating them at 110 °C for 24 h. Bulk compositions in terms of X_Y = Y/Ce + Y of each individual experiment are shown in Figure 2 along with the respective temperature and pressure experiment conditions (see also Table 1).

Experimental procedure

Experiments at 2 kbar were performed in standard cold-seal vessels with water as pressure medium. The temperature was recorded continuously and measured with shielded chromel-alumel thermocouples inside the pressure vessel next to the sample. The maximum temperature gradient along the capsule was ±2 °C and the

TABLE 1. Experimental conditions, bulk compositions, and compositions of monazite and zenotime obtained by XRD and EMP

Experiment No.	P (kbar)	T (°C)	Duration (h)	Bulk composition		Composition of run products							
						Monazite				Xenotime			
				X_{Ce}	X_Y	Cell volume	Err (σ)	X_Y (XRD)	X_Y (EMP)	Cell volume	Err (σ)	X_Y (XRD)	X_Y (EMP)
P16	2	700	408	1.00	0.00	300.84	0.12	0.000	n.d.			—	—
P17	2	700	408	0.00	1.00			—	—	285.28	0.12	1.000	n.d.
P13	2	950	30	0.85	0.15	297.05	0.12	0.150	n.d.			—	—
P14	2	950	30	0.90	0.10	298.21	0.10	0.100	n.d.			—	—
P15	2	950	30	0.95	0.05	299.57	0.10	0.050	n.d.			—	—
P1	2	1000	19	0.40	0.60	296.53	0.25	0.167	0.155	285.70	0.25	0.988	n.d.
P2	2	900	69	0.40	0.60	297.62	0.24	0.125	0.139	285.60	0.22	0.991	0.975
P3	2	800	624	0.10	0.90	298.08	0.26	0.107	0.137	285.81	0.27	0.985	0.993
P5	2	700	88	0.20	0.80	299.15	0.22	0.066	0.080	286.37	0.20	0.968	0.970
P6	2	700	312	0.80	0.20	298.94	0.25	0.074	0.080	286.26	0.24	0.972	0.978
P7	2	700	88	0.40	0.60	298.99	0.20	0.072	n.d.	286.23	0.20	0.972	0.970
P8	2	700	312	0.60	0.40	299.05	0.20	0.070	n.d.	286.23	0.19	0.972	n.d.
P9	2	600	552	0.60	0.40	299.28	0.26	0.061	n.d.	286.56	0.28	0.963	n.d.
P10	2	600	490	0.80	0.20	299.31	0.21	0.060	0.053	286.60	0.30	0.962	0.982
P12	2	500	504	0.80	0.20	299.57	0.23	0.050	0.045	285.53	0.27	0.993	0.990
P60	2	400	816	0.80	0.20	299.88	0.20	0.038	n.d.	285.63	0.19	0.990	n.d.
P61	2	400	816	0.20	0.80			n.d.	n.d.	285.49	0.20	0.994	n.d.
P62	2	300	816	0.80	0.20	300.09	0.20	0.030	n.d.	285.53	0.20	0.993	n.d.
P63	2	300	816	0.20	0.80			n.d.	n.d.	285.53	0.19	0.993	n.d.
P68	5	800	19	0.80	0.20	297.62	0.21	0.125	n.d.	285.53	0.21	0.993	n.d.
P69	5	800	19	0.20	0.80			n.d.	n.d.	285.53	0.18	0.993	n.d.
P66	10	800	25	0.80	0.20	297.10	0.19	0.145	n.d.	285.83	0.24	0.984	n.d.
P21	15	900	26	0.20	0.80			n.d.	n.d.	285.88	0.23	0.983	n.d.
P22	15	900	26	0.80	0.20	295.70	0.19	0.199	n.d.				
P23	15	800	40	0.20	0.80			n.d.	n.d.	285.56	0.22	0.992	n.d.
P24	15	800	40	0.80	0.20	296.45	0.18	0.170	n.d.	285.83	0.24	0.984	n.d.
P25	15	700	88	0.20	0.80			n.d.	n.d.	286.02	0.19	0.979	n.d.
P26	15	700	88	0.80	0.20	297.12	0.15	0.144	n.d.	285.56	0.15	0.992	n.d.
P27	15	600	72	0.20	0.80			n.d.	n.d.	285.35	0.25	0.998	n.d.
P28	15	600	72	0.80	0.20	298.19	0.23	0.103	n.d.	285.56	0.23	0.992	n.d.
P30	15	500	115	0.80	0.20	298.58	0.21	0.088	n.d.	285.81	0.20	0.985	n.d.
P64	15	400	66	0.80	0.20	298.76	0.19	0.081	n.d.	285.53	0.20	0.993	n.d.

Notes: Y concentrations of all monazites of the two-phase experiments were determined by XRD using the volume calibration curve of the single phase experiments P13 to P16 (see Fig. 5). Errors in $X_Y^{monazite}$ determined by XRD are about ±0.01. For errors by EMP see Figure 6. Ce concentrations of all xenotime of the two-phase experiments were determined by XRD using the cell volume of pure xenotime produced in experiment P17 along with the estimated volume of the theoretical $CePO_4$ end-member in the xenotime structure (Ni et al. 1995, and explanation in the text). Errors in $X_Y^{xenotime}$ are also about ±0.01.

maximum error in temperature ±3 °C. The pressure was measured using a pressure transducer calibrated against a Heise gauge manometer, and the quoted pressure is accurate to ±50 bars. Experiment durations were between 19 and 816 h. Experiments at 5, 10, and 15 kbar were performed in a non-endloaded piston-cylinder apparatus with a 22 mm diameter pressure chamber and NaCl as pressure medium under piston-in conditions. Pressure was recorded continuously and controlled within 0.1 kbar nominal. Pressure calibrations gave a maximum error in pressure measurement of ±600 bars based on our calibration of the reaction albite = jadeite + quartz between 12 and 22 kbar. For temperature control, sheathed Ni-Cr-Ni thermocouples were used, uncorrected for pressure. Temperatures were recorded automatically. Measurements of the T gradient along the capsule indicated that the accuracy was ±5 at 700 °C, and ±8 at 900 °C. Experiment durations of piston cylinder experiments were between 19 and 115 h. Cold-seal vessels were quenched with compressed air to room temperature within about 3 min. Piston-cylinder experiments were quenched within a few seconds by a water-cooled jacket. The weight of each capsule was checked after quenching. Any capsules that showed significant weight loss were discarded. After opening the capsule, excess H_3PO_4 was removed by washing with distilled water, and the powder was dried. Finally, the product powders were split up for optical microscopy, scanning electron microscopy, electron microprobe, and X-ray powder diffraction investigations.

Electron microprobe analysis and X-ray powder diffractometry

The product powders were embedded into epoxy resin and polished. Analyses of the phosphates were obtained with the use of an automated CAMECA SX50 electron microprobe equipped with a wave-length dispersive system. Operating conditions were 15 kV, 10 nA on the Faraday cup, with a beam diameter of 1 μm and 20 sec of integration time. The background was measured 10 sec at each side of the peak. For Ce and Y we used the $L\alpha_1$ line, for P the $K\alpha_1$ line, and as standards synthetic $CePO_4$ and YPO_4 using the PAP correction procedure. Of seven experimental products, an extensive set of about 40 EMP analyses of each phase was produced. Analyses were ac-

cepted if the oxide sum was 100 ± 1.5 wt% and if P and ΣCe + Y were 1 ± 0.015 cfu, assuming four O atoms.

We were not, however, able to produce an EMP data set of satisfactory quality. Apparent Ce and Y concentrations were broadly scattered. We believe this to be an analytical artifact because of the very small dimensions (3 to 10 μm) of the phosphate grains rather than true inhomogeneities in either set of minerals. This is strongly supported by sharp individual X-ray reflections of monazite and xenotime that show no asymmetry. There is thus strong evidence for an absence of compositional zonation. Monazite and xenotime compositions derived from X-ray diffraction proved to be more reliable. A comparison between EMP- and X-ray data with associated errors is given below.

All product powders were investigated with a focusing STOE X-ray powder-diffractometer Stadi P using Cu$K\alpha_1$ radiation and a position-sensitive detector with a peak resolution of 0.05° with respect to 2θ. Peak positions were calibrated daily using the NBS SRM-640b external silicon standard. The unit-cell refinements were performed using the Rietveld-refinement program of the GSAS software package (Larson and Von Dreele 1988). The relative proportions of monazite and xenotime were different for each experiment, depending on the bulk composition chosen (Fig. 2). Although both phases were refined simultaneously, the majority phase was preferentially used for the unit-cell refinements. The relationships between lattice constants and composition of REE-phosphate solid solutions is outlined below.

Results

The product powders from all experiments consisted exclusively of monazite and xenotime. No other solid phases were present. Crystals are generally euhedral, <1 to 10 μm in size. Monazite and xenotime are easily distinguishable by their monoclinic and tetragonal morphologies (Fig. 3). The experimental conditions, bulk compositions, and compositions of monazite and xenotime obtained by XRD and EMP of 32 experiments are given in Table 1.

Determination of monazite and xenotime composition

Experiment no. P16 and P17 produced pure $CePO_4$ and YPO_4, consistent with the end-member bulk compositions. The unit-cell volume of pure $CePO_4$ is 300.84 (12) Å^3 in agreement with the value of 300.60 Å^3 given by Pepin et al. (1981; also from powder XRD data) but somewhat different from the value of 299.49 Å^3 given by Ni et al. (1995; from single crystal XRD data). Experiments P15 (X_Y^{bulk} = 0.05), P14 (X_Y^{bulk} = 0.10), and P13 (X_Y^{bulk} = 0.15), all synthesized at 950 °C and 2 kbar, yielded only monazite without xenotime, thus representing a one phase region in *PTX* space (see Fig. 2). Unit-cell parameters of $(Ce,Y)PO_4$ monazite correlate strongly with composition. It is then reasonable to use the X_Y–cell-volume relationship of these single phase experiments as a calibration curve for the determination of monazite compositions synthesized in the two-phase region. Figure 4 shows the variation in the unit-cell parameters (*a, b, c, V,* and *β*) with Y concentration of monazite synthesized in the one-phase region. There is a strong linear decrease in *a, b, c,* and *V* and increase in *β* with increasing incorporation of the smaller Y^{3+} ion into the monazite structure (Table 2). The linear least-squares regression of the data gives the following calibrations: $a = 6.800 - 0.194\ X_Y$, $b = 7.027 - 0.222\ X_Y$, and $c = 6.474 - 0.142\ X_Y$ (Å), $\beta = 103.46 + 0.64\ X_Y$ (°), and $V = 300.83 - 25.5\ X_Y$ (Å^3). For the X_Y–cell-volume curve, errors of ± 0.10 Å^3 (1σ) for monazites of P13 to P16 (Table 1) result in errors in X_Y of about ± 0.005 (Fig. 4d).

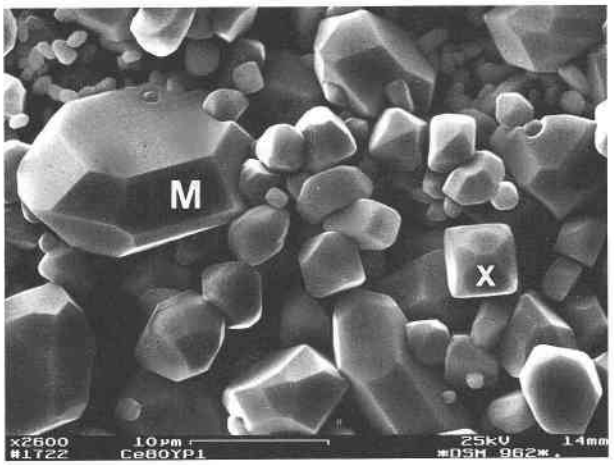

FIGURE 3. Scanning electron microscope micrograph of experiment no. 6 (700 °C, 2 kbar). Most crystals are euhedral. Monazite (M) and xenotime (X) crystals are easily distinguishable by their morphology. Monazite has a monoclinic and xenotime a tetragonal external shape.

The composition of monazite in each two-phase experiment was determined using the above calibration of lattice parameters. Lattice parameters in terms of $V^{1/3}$ (Å) and the corresponding composition of monazite for each experiment are given in Table 1 and Figure 5. The error in determining the cell volume of monazite in two phase products is about ± 0.2 Å^3 (1σ), resulting in errors in X_Y of about ± 0.01. Table 1 also contains the results of EMP analyses for monazites from seven selected two phase experiments. The comparison of X_Y of monazite obtained by XRD with X_Y determined by EMP analyses is shown in Figure 6. The results of both methods show overall agreement, however, the EMP data are broadly scattered with an error 1σ being about five times larger. We believe that these inaccuracies in the EMP data are due to an analytical artifact that arises from both the very small grain sizes (3 to 10 μm) as well as analytical interferences of closely packed monazite and xenotime grains in the grain mount and do not result from monazite inhomogeneities. This is supported by the fact that X-ray reflections of monazite solid solutions synthesized in the one- and two-phase fields show identical half widths as reflections of pure $CePO_4$ end-member (Fig. 7). That EMP inaccu-

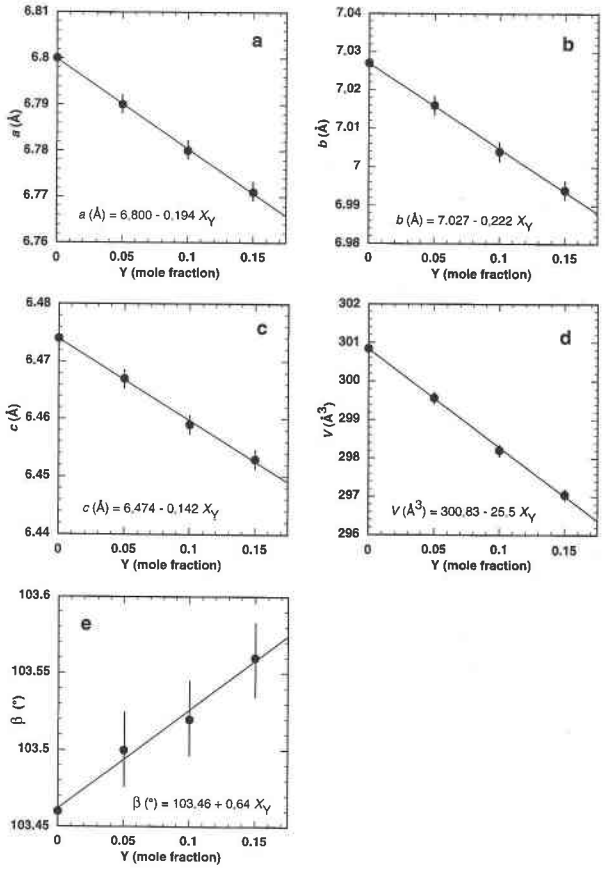

FIGURE 4. Variation in the *a, b, c, V,* and *β* unit-cell parameters (**a–e**, respectively) vs. Y concentration of monazite synthesized in the one phase region (experiment numbers 13, 14, 15, and 16). The lines are least square regressions and their equations are also given. Error bars denote 1σ errors. Values are from Table 2.

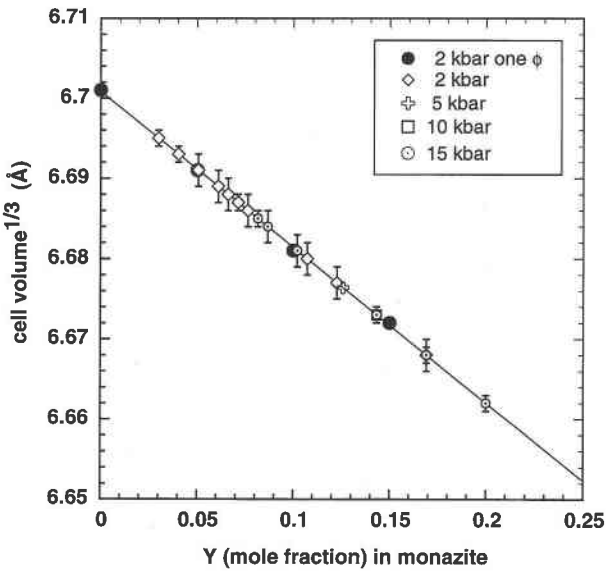

FIGURE 5. Plot of volume ($V^{1/3}$) vs. Y concentration of monazites. Y concentrations of all monazites of the two phase experiments were determined using the volume calibration curve obtained by the single phase experiments (black dots with regression line, see also Fig. 4). Error bars from X-ray diffraction are 1σ errors resulting in errors of X_Y of about ± 0.01. Volume values are from Table 1.

racies are due to small grain sizes is further supported by synthesis experiments in the (Ce,Y,Gd)$(PO)_4$ ternary system (R. Gratz and W. Heinrich, in preparation). There, grain sizes were in the range of 10 to 20 μm, and the EMP data were much less scattered, allowing accuracy of ±0.015 mol% of each REE in monazite solid solutions of the (Ce,Y,Gd)$(PO)_4$ ternary. In the binary system, the XRD data are more accurate, and we use these data for inferring the compositional relationships between the two phases in *PTX* space.

The cell volume of pure YPO_4 (xenotime) produced in experiment P17 is 285.28 ±0.12 Å^3 (Table 1). The determined cell volumes of xenotime from all two-phase experiments range from 285.35 ± 0.25 Å^3 (experiment P27) to 286.60 ± 0.30 Å^3 (experiment P10), and most of them are between 285.35 and 286.0 Å^3. The increase in volume is very small and exceeds the 1σ error in volume determination only by a factor of two to three. It is obvious that only a very small amount of Ce is incorporated into xenotime. The calibration of an X_{Ce}–volume curve by means of xenotime single-phase experiments is therefore unreasonable. Instead, we used the linear extrapolation of the $r(REE^{3+})$–volume curve for pure $REEPO_4$ in xenotime structure (see Fig. 1) along with the ion radius of 1.143 Å of Ce^{3+} in eightfold coordination (Shannon 1976) and estimated the unit-cell volume of a hypothetical $CePO_4$ end-member in xenotime structure as 321.35 Å^3. Xenotime compositions in terms of $X_Y^{xenotime}$ (Table 1) were then determined with the assumption of a linear volume increase between YPO_4 and hypothetical $CePO_4$ in xen-

TABLE 2. Variation in the *a, b, c, V,* and β unit-cell parameters of monazites from the single phase experiment products (experiment numbers P13 to P16)

Experiment No.	Composition	*a* (Å)	*b* (Å)	*c* (Å)	β (°)	*V* (Å^3)
P13	$(Ce_{0.85}Y_{0.15})PO_4$	6.771(1)	6.994(1)	6.453(1)	103.56(3)	297.05(12)
P14	$(Ce_{0.90}Y_{0.10})PO_4$	6.780(1)	7.004(1)	6.459(1)	103.52(3)	298.21(10)
P15	$(Ce_{0.95}Y_{0.05})PO_4$	6.790(1)	7.016(1)	6.467(1)	103.50(3)	299.57(10)
P16	$CePO_4$	6.800(1)	7.027(1)	6.474(1)	103.46(2)	300.84(12)

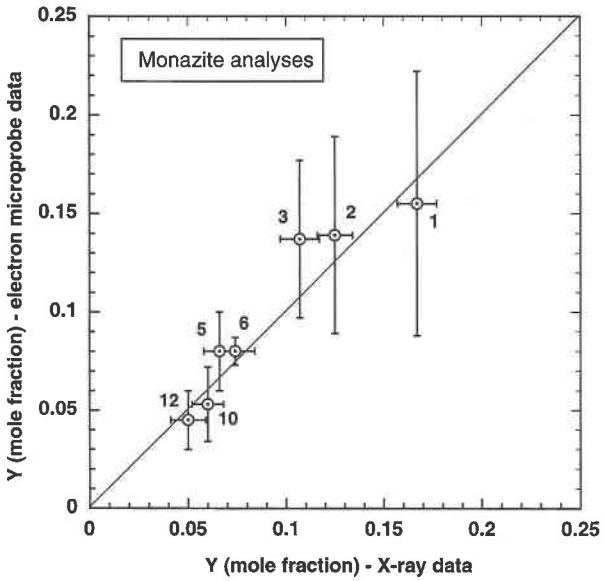

FIGURE 6. Y concentrations of monazite obtained by electron microprobe vs. X-ray diffraction results from seven selected experiments (numbers from Table 1) with error bars (1σ). Although there is reasonable agreement between both data sets, the XRD results are more accurate.

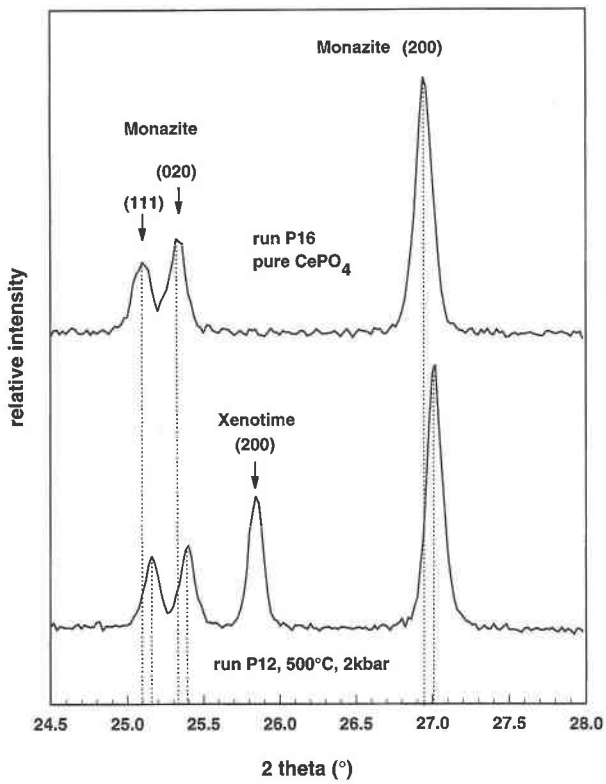

FIGURE 7. Portion of the X-ray patterns of experiment P16 (pure $CePO_4$ end-member) and P12 (coexisting monazite and xenotime). The (111), (020), and (200) reflections of monazite show identical half width. Peaks of P12 are shifted to higher 2θ values because of incorporation of 5 ± 1 mol% Y into the monazite structure. The pattern of P12 shows also the (200) reflection of xenotime.

otime structure. Resulting X_Y values of all experiments range between 0.97 and 0.99, except experiments P9 and P10 ($X_Y \approx 0.96$), with an error of about ± 0.015. X_Y values of xenotime determined by EMP from seven selected experiments fall into the same envelope (Table 1) with analytical errors in the same range.

The $CePO_4$-YPO_4 miscibility gap

The compositions of monazite coexisting with xenotime at various temperatures and pressures are shown in an $X_Y^{monazite}$-temperature plot (Fig. 8). All data are from Table 1. The experiments define two monazite limbs of the miscibility gap of the $CePO_4$-YPO_4 binary at 2 and 15 kbar, respectively, over a temperature range of 300–1000 °C. At 2 kbar, Y concentrations in monazite increase from 3 mol% at 300 °C to 17 mol% at 1000 °C. At 15 kbar, Y concentrations are 6 mol% at 300 °C and increase up to about 25 mol% at 1000 °C. The results are consistent within the analytical error limits of ± 1 mol% Y. Figure 9 shows the pressure dependence of Y incorporation into monazite coexisting with xenotime at 800 °C. Y concentrations increase from 10 mol% at 2 kbar to 17 mol% at 15 kbar. Within analytical error, the pressure dependence at 800 °C can be approximated by a linear function (straight line in Fig. 9). Combining all PTX_Y data, the position of the monazite limb of the miscibility gap boundary in *PTX* space for the relevant *P-T* conditions is fitted by

$$X_Y^{monazite} = \frac{(1.459 + 0.0852\,P)\,e^{0.002274T}}{100} \qquad (1)$$

where P is in kbar and T is in °C.

The corresponding $X_Y^{xenotime}$-temperature plot of xenotime compositions coexisting with monazite is shown in Figure 10. For the vast majority of experiments, Y concentrations of xenotime range between 98 and 99 mol%. Given our analytical error of $\pm$ 1.5 mol% in Y (see inset of Fig. 10), it is not possible to derive a temperature or pressure dependence for the xenotime limb. The mean X_Y value of 0.98 ± 0.015 is covered by all experiments with only two exceptions (experiments P9 and P10, both at 600 °C and 2 kbar, with relatively large errors in *V*, see Table 1). Whichever number may be correct, it is obvious that only a very small amount of Ce is incorporated in xenotime and that the *P-T* dependence of this incorporation is, if present at all, very small.

The shape of the $CePO_4$-YPO_4 miscibility gap is strongly asymmetric, and our binary resembles the calcite-dolomite solvus in many aspects (Goldsmith and Newton 1969; Gottschalk and Metz 1992). Both the calcite limb of the carbonate system and the monazite limb of the phosphate system strongly depend on temperature and are useful for geothermometry, whereas the dolomite and xenotime limbs are not. The main difference between the two systems is that the position of the monazite limb

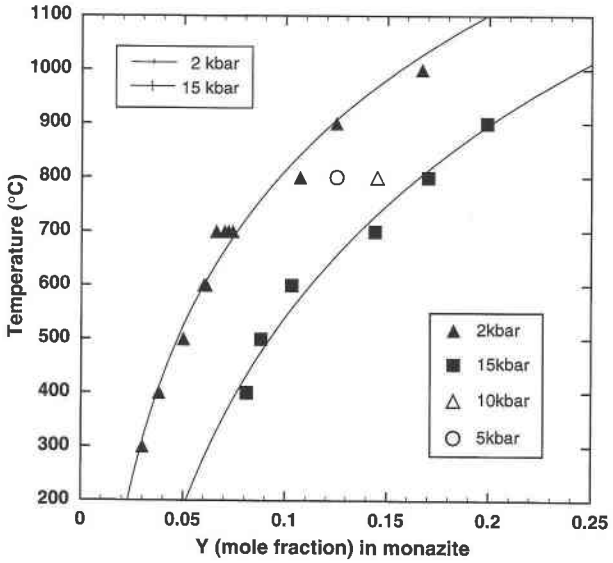

FIGURE 8. $X_Y^{monazite}$-temperature plot depicting the monazite limb of the monazite–xenotime miscibility gap at 2 kbar (black triangles) and 15 kbar (black squares). All data points are from reaction products that contained monazite plus xenotime. Values are from Table 1.

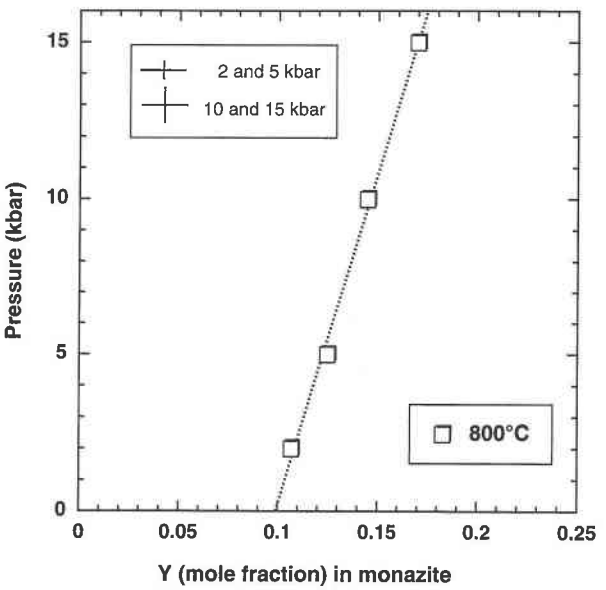

FIGURE 9. $X_Y^{monazite}$-pressure plot depicting the pressure dependence of the monazite limb of the miscibility gap at 800 °C. Data points are from reaction products that contained monazite plus xenotime. Values are from Table 1.

also depends on pressure, whereas variation of the position of the calcite limb with pressure is very small (Gottschalk and Metz 1992). Aside from that, the miscibility gap in the calcite-dolomite binary is a true solvus because both phases are isostructural. Monazite and xenotime are not, and therefore we prefer here the term "miscibility gap" (see Putnis 1992; Spear 1993 p. 87).

Discussion

The $CePO_4$-YPO_4 binary—an appropriate model system for monazite-xenotime pairs in metamorphic rocks?

The compositions of coexisting monazite and xenotime from a suite of seven metapelites that crystallized between 400–700 °C at pressures from about 3 to 5 kbar revealed that the major element concentrations of both are independent of metamorphic grade and are only due to bulk rock composition (Heinrich et al. 1997). A typical pattern of REE + Y concentrations is shown for lower granulite facies sample Tb 132 (Fig. 11). Major components of monazite are La (X_{La} = 0.20), Ce (X_{Ce} = 0.41), and Nd (X_{Nd} = 0.17). All other REE, Ca, and Th are ≤6 mol% (data from Heinrich et al. 1997), and these are very similar to monazite compositions reported from other metapelites (Kingsbury et al. 1993; Suzuki et al. 1994). Xenotime consists mainly of Y (X_Y = 0.80) plus some Dy, Er, Yb, and Gd, all in the range of about 5 mol% (Fig. 11). The LREE with large ionic radii (La to Sm) are preferentially partitioned into monazite, and the HREE with smaller radii (Gd to Yb) are partitioned into xenotime. Of these, only Y, Gd, and Dy ($X_{Y + Gd + Dy}$ = 0.10 in Tb 132) are prominent minor elements in monazite, and in xenotime only Sm and Nd are minor ($X_{Sm + Nd}$ = 0.01 in Tb 132; Fig. 11).

The essential point is that incorporation of the HREE (Gd to Yb) into monazite and of LREE (La to Sm) into xenotime for metapelitic bulk compositions turned out to be temperature dependent (Heinrich et al. 1997). This is

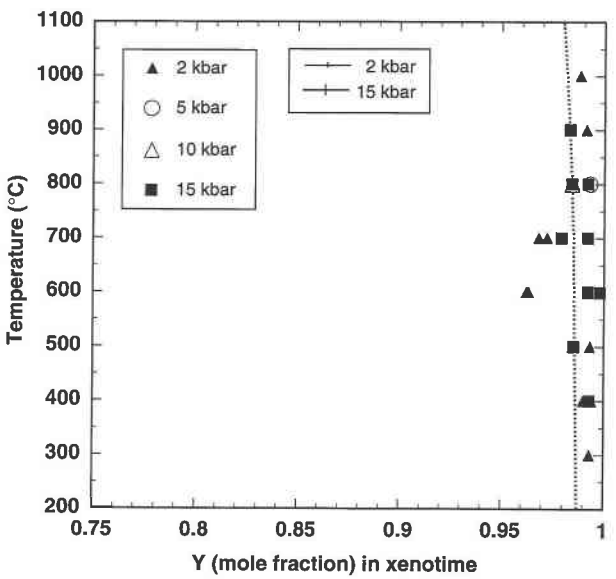

FIGURE 10. $X_Y^{xenotime}$-temperature plot depicting the xenotime limb of the monazite–xenotime miscibility gap at 2 kbar (black triangles) and 15 kbar (black squares). All data points are from reaction products that contained moazite plus xenotime. Values are from Table 1.

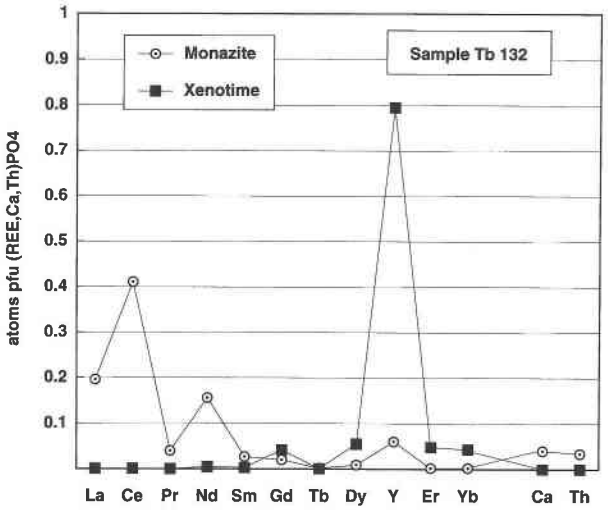

FIGURE 11. REE + Y, Ca, and Th contents of coexisting monazite and xenotime, given per formula unit. The sample Tb 132 is from a lower granulite facies metapelite that equilibrated at peak metamorphic conditions of about 700 °C and 5 kbar. Analyses from Heinrich et al. (1997, their Table 1).

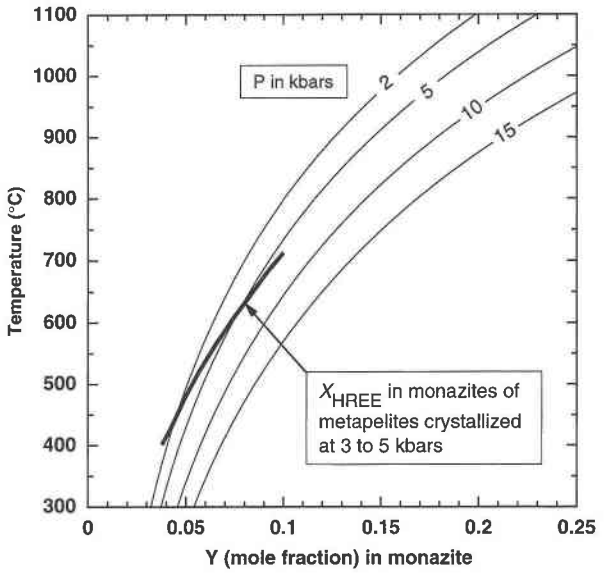

FIGURE 12. $X_Y^{monazite}$-temperature plot showing the monazite limb of the miscibility gap at various pressures, calculated using Equation 1. Thick curve indicates the mole fraction of Y + HREE (Gd-Lu) of natural monazites from a metapelite suite that crystallized together with xenotime at about 400–700 °C and about 3 to 5 kbar (Heinrich et al. 1997). The monazite limb of the (Ce-Y)PO_4 binary and that of the (LREE-HREE,Y)PO_4 system in rocks almost coincide within error limits (see Fig. 7).

shown in Figures 12 and 13, along with the experimentally determined miscibility gap boundaries of the $CePO_4$-YPO_4 binary. The $X_{HREE}^{monazite}$-temperature curve, empirically calibrated at 400–700 °C and about 3 to 5 kbar, almost coincides with the $X_Y^{monazite}$ vs. temperature binary limbs at 2 and 5 kbar, calculated using Equation 1 (Fig. 12). Similarly, the empirically determined xenotime limb coincides with that of the binary, given that the error in $X_Y^{xenotime}$ from our experiment is not better than ± 0.015 (Fig. 13). Thus, the $CePO_4$-YPO_4 binary represents an adequate model system for natural monazite-xenotime pairs, at least for metapelitic bulk compositions.

A simple explanation for the similarity of the experimentally derived and the natural monazite limbs of the miscibility gap is that the average effective ionic radii of monazite solid solutions from metapelites are very similar to that of synthetic monazite in the simple binary system. Ce^{3+} in ninefold coordination has an effective ionic radius of 1.196 Å (Shannon 1976; see also Ni et al. 1995, and Fig. 1) and incorporation of 10 mol% Y (effective radius in ninefold coordination = 1.075; Shannon 1976) would result in an average radius of only 1.184 Å and volume reduction from 300.84 Å to 299.57 $Å^3$ for $Ce_{0.9}Y_{0.1}PO_4$ solid solutions (Fig. 4 and Table 2). Taking the compositions of the monazites from the seven metapelites (Heinrich et al. 1997; their Table 1) and assuming ionic radii of ninefold coordination (Shannon 1976), their average effective radii values range from 1.178 Å to 1.185 Å. Thus, $CePO_4$ is a good representative for monazite of complex composition as is YPO_4 for xenotime, the latter being evident from Figure 11. However, a more detailed understanding of the multivariate (LREE-HREE,Y)PO_4 system must await thermodynamic data on pure (REE,Y)PO_4 phases.

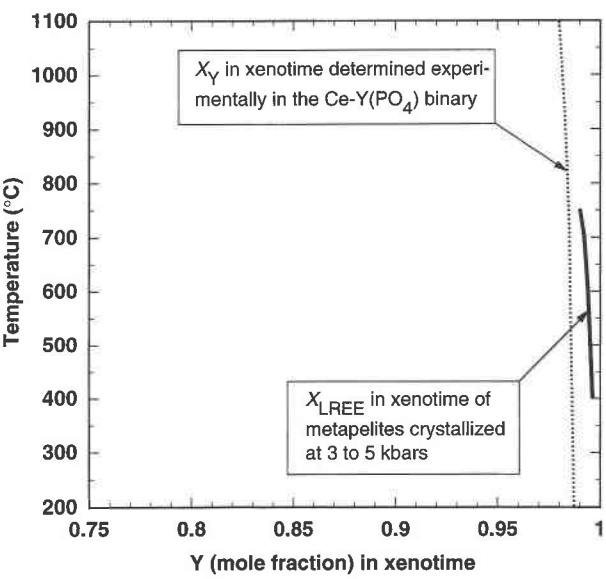

FIGURE 13. $X_Y^{xenotime}$-temperature plot showing the xenotime limb derived from our experiments along with the mole fractions of LREE (La-Sm) of monazite from a metapelite suite that crystallized together with monazite at 400–700 °C (thick curve). Note that the experimentally determined limb has an error of ± 0.015 in X_Y. Within that error, both curves coincide.

The monazite-xenotime geothermobarometer

It has been suggested that monazite is unstable in very low- to low-grade metamorphic rocks relative to other minerals such as bastnaesite, apatite, or REE-bearing epidote (Smith and Barreiro 1990; Ohr et al. 1994; Schaltegger et al. 1994). There are apparently no simple reactions that might control monazite and xenotime stability in low-grade rocks. Heinrich et al. (1997) found stable monazite-xenotime pairs in metapelites that equilibrated at about 400 °C and 3 kbar, and in our experiments coexisting monazite and xenotime formed at 300 °C up to 1000 °C at both low and high pressures. It is most likely that (REE + Y)PO_4 phases are stable up to 1400 °C at low pressures (J.M. Montel, personal communication). In conclusion, the monazite-xenotime geothermobarometer can be applied, in principle, over the entire range of *P-T* conditions where monazite and xenotime are stable in metamorphic rocks.

The most useful application of the monazite–xenotime miscibility gap to metamorphic rocks is thermometry using the compositions of monazite that coexist with xenotime for rocks of known pressure. Monazite in medium- to high-grade rocks often shows prograde growth zonation, and there is no indication of retrograde resetting with respect to REE concentrations (DeWolf et al. 1993, Zhu et al. 1994; Heinrich et al. 1997; C.P. DeWolf and E. Essene, in preparation). Thus, monazite compositions are indicative of temperatures at which monazite grew. Furthermore, monazite is often used for U-Pb age determinations because of its high U and Pb contents (Parrish 1990). Recent isotopic studies have shown that the effective closure temperature for the U-Pb system in monazite is >700 °C (Smith and Barreiro 1990; DeWolf et al. 1993; Zhu et al. 1994; Suzuki et al. 1994) and that monazite may preserve ages corresponding to peak temperatures up to the granulite facies and may even record prograde growth ages. If so, our thermometer has the potential of determining peak metamorphic temperatures and corresponding ages on one mineral, which was up to now only possible for garnet. In the case of prograde zoning of monazite, the dating of different domains of a zoning profile along with application of the thermometer provides a promising tool for determining prograde branches of *PTt* paths. Moreover, the high Nd and Sm contents of monazite and xenotime and the strong partitioning of Sm/Nd in xenotime over monazite (Heinrich et al. 1997, their Table 1; see also Fig. 11) may provide two-mineral Sm-Nd isochrons, and with our thermometer, the obtained ages could be again linked directly to their growth temperatures. Thus, the (REE,Y)PO_4 phases have an enormous potential in deriving metamorphic *PTt* paths.

Acknowledgments

We gratefully acknowledge the assistance of R. Schulz during the performance of the experiments. Thanks go also to D. Rhede and O. Appelt for providing EMP facilities, and U. Glenz and I. Bauer for help with SEM and XRD analyses. We also thank E.M. Schemmert who made the grain mounts. G. Franz (TU Berlin) and D. Harlov critically read an earlier version of the manuscript. Helpful comments of D. London and P. Nabelek improved the paper.

References cited

DeWolf, C.P., Belshaw, N., and O'Nions, R.K. (1993) A metamorphic history from micron-scale $^{207}Pb/^{206}Pb$ chronometry of Archean monazite. Earth and Planetary Science Letters, 120, 207–220.

Franz, G., Andrehs, G., and Rhede, D. (1996) The crystal chemistry of natural monazite and xenotime from metamorphic rocks—a case study from the Saxothuringian-Moldanubian area in NE Bavaria, Germany. European Journal of Mineralogy, 8, 1097–1118.

Goldsmith, J.R. and Newton, R.C. (1969) *P-T-X* relations in the system $CaCO_3$-$MgCO_3$ at high temperatures and pressures. American Journal of Science, 267, 160–190.

Gottschalk, M. and Metz, P. (1992) The system calcite-dolomite: a model to calculate the Gibbs free energy of mixing on the basis of existing experimental data. Neues Jahrbuch Mineralogie Abhandlungen, 164, 29–55.

Heinrich, W., Andrehs, G., and Franz, G. (1997) Monazite—xenotime miscibility gap thermometry. I. An empirical calibration. Journal of Metamorphic Geology, 15, 3–17.

Kingsbury, J.A., Miller, C.F., Wooden, J.L., and Harrison, T.M. (1993) Monazite paragenesis and U-Pb systematics in rocks of the eastern Mojave Desert, California, U.S.A.: implications for thermochronometry. Chemical Geology, 110, 147–167.

Larson, A.C. and Von Dreele, R.B. (1988) GSAS—Generalized structure analysis system. Los Alamos National Laboratory Report LAUR 86-748, 1–150.

Ni, Y., Hughes, J.M., and Marino, A.N. (1995) Crystal chemistry of the monazite and xenotime structures. American Mineralogist, 80, 21–26.

Ohr, M., Halliday, A.N., and Peacor, D.R. (1994) Mobility and fractionation of rare earth elements in argillaceous sediments: implications for dating diagenesis and low-grade metamorphism. Geochimica et Cosmochimica Acta, 58, 289–312.

Parrish, R.R., 1990. U-Pb dating of monazite and its application to geological problems. Canadian Journal of Earth Science, 27, 1431–1450.

Pepin, G.J. and Vance, E.R. (1981) Crystal data for rare earth orthophosphates of the monazite structure-type. Journal of Inorganic Nuclear Chemistry, 43, 2807–2809.

Putnis, A. (1992) Introduction to Mineral Sciences, 457 p. Cambridge University Press, Cambridge, U.K.

Schaltegger, U., Stille, P., Rais, N., Piqué, A., and Clauer, N. (1994) Neodymium and strontium isotopic dating of diagenesis and low grade metamorphism of argillaceous sediments. Geochimica et Cosmochimica Acta, 58, 1471–1481.

Shannon, R.D. (1976) Revised effective ionic radii and systematic studies of interatomic distances in Halides and Chalcogenides. Acta Crystallographica, A32, 751–767.

Smith, H.A. and Barreiro B. (1990) Monazite Ub-Pb dating of staurolite grade metamorphism in pelitic schists. Contributions to Mineralogy and Petrology, 105, 602–615.

Spear, F.S. (1993) Metamorphic phase equilibria and pressure-temperature-time paths. Mineralogical Society of America, Washington, 799 p.

Suzuki, K., Adachi, M., and Kajizuka, I. (1994) Electron microprobe observations of Pb diffusion in metamorphosed detrital monazites. Earth and Planetary Science Letters, 128, 391–405.

Zhu, X.K., O'Nions, R.K., and Reed, S.J.B. (1994) REE distribution patterns of monazite: constraint on monazite origin in metamorphic rocks. 16th General Meeting IMA, Pisa, Abstract Vol., 461.

Manuscript received September 30, 1996
Manuscript accepted February 13, 1997